✕USCAP

ARTICLE

Frequent overexpression of klotho in fusion-negative phosphaturic mesenchymal tumors with tumorigenic implications

Cheng-Han Lee[1] · Sheng-Yao Su[2,3] · Kesavan Sittampalam[4] · Paul Chih-Hsueh Chen[5] · Fredrik Petersson[6] ·
Yu-Chien Kao[7] · Thomas O. Carpenter[8] · Tsung-Han Hsieh[9] · Eiichi Konishi[10] · Jen-Wei Tsai[11] · Steven D. Billings[12] ·
Andrew L. Folpe[13] · Jen-Chieh Lee [14]

Abstract

Phosphaturic mesenchymal tumors (PMT) are tumors that cause hypophosphatemia/osteomalacia chiefly by secreting FGF23. We have identified *FN1-FGFR1/FGF1* fusion genes in nearly half of PMT, suggesting a central role of FGFR1 pathways in the pathogenesis of PMT. Tumorigenic drivers are unknown for tumors where previous study detected neither fusion, including many in bone, where FISH failed because of tissue decalcification. To identify alternative fusions in PMT without known fusions, as well as to validate the positive FISH results and characterize the fusion junctions, 34 PMT were studied, including 12 with known *FN1-FGFR1* fusion by FISH (Group A), 2 with *FN1-FGF1* (B), 12 with neither fusion (C), and 8 with previous acid-based decalcification and hence unknown fusion status (D). In total, 23 archival samples were subjected to anchored multiplex PCR-based RNA-sequencing (AMP-seq) with primers targeting *FN1*, genes encoding the FGF/FGFR families, and *KL* (α-Klotho); five Group C cases were also studied with whole-transcriptomic and exome-captured RNA sequencing, respectively. The AMP-seq results were consistent with previous FISH and/or transcriptomic sequencing data, except in one old Group A sample. One case had a novel *FGFR1* exon 9 breakpoint, confirmed by genomic DNA sequencing. One Group D bone tumor was found to harbor *FN1-FGF1*. All 3 RNA-sequencing platforms failed to identify convincing fusion genes in Group C (N = 10), which instead expressed significantly higher levels of either *KL* or *KLB*. This result was further confirmed with *KL* and *KLB* RNA CISH semi-quantification (RNAscope). Our results demonstrated the utility of AMP-seq, which was compromised by decalcification and prolonged archiving. Of potential importance, fusion-negative PMT frequently overexpressed α-Klotho (or instead β-Klotho less commonly), whose role as an obligatory co-receptor for FGF23-FGFR1 binding suggests its aberrant expression in osteocytes/osteoblasts might result in an FGF23-FGFR1 autocrine loop that in turn drives the overexpression of FGF23 and tumorigenesis through activated FGFR pathways.

Introduction

Phosphaturic mesenchymal tumors (PMT) are uncommon bone or soft tissue neoplasms that cause hypophosphatemia and osteomalacia by secreting a variety of circulating phosphatonins, particularly fibroblast growth factor 23 (FGF23) [1–7]. By characterizing a large series of cases using RNA sequencing and fluorescence in situ hybridization (FISH), we have previously identified *FN1-FGFR1* or *FN1-FGF1* fusion genes in nearly half of PMT, thus shedding light on the potentially pivotal roles of the fibroblast growth factor 1 (FGF1)-fibroblast growth factor receptor 1 (FGFR1) axis, as well as the interaction between *FN1*-encoded fibronectin and other extracellular matrix molecules, in the tumorigenesis of PMT [8, 9]. The tumorigenic drivers remain obscure, however, for the other cases in which FISH detected neither fusion gene, as well as a significant subset of bone tumors where FISH failed, probably as a result of extensive DNA degradation due to acid-based decalcification. It is unknown whether

✉ Jen-Chieh Lee
   leejenchieh@ntuh.gov.tw

Extended author information available on the last page of the article

alternative fusion genes, especially those involving the other fibroblast growth factor receptors or fibroblast growth factors, could be responsible for cases negative for both previously identified fusions. Also noteworthy is a patient (case PMT-61 in this series) with a germline rearrangement involving the upstream of the *KL* gene (coding for α-Klotho) which resulted in its upregulation; the patient developed hypophosphatemic rickets early in life, with 2 PMT identified at the age of 30, neither of which contained either fusion [9, 10]. Whether overexpression of *KL* plays a tumorigenic role in other PMT, particularly in those fusion-negative tumors as an alternative to *FN1-FGFR1/FGF1* fusions, remains to be determined.

Although formalin-fixed and paraffin-embedded (FFPE) tissue specimens represent by far the predominant repository of archived clinical samples, RNA sequencing on FFPE samples has been substantially limited by the highly degraded nature of RNA [11]. Methods to enrich the coding regions in the transcriptome libraries have achieved some success, including the exome capture and anchored multiplex PCR (AMP) techniques [12–14]. However, the decalcification of FFPE bone specimens adds yet another level of challenge. The conventional acid-based decalcification process confers extensive disruption to the nucleic acids, greatly hindering molecular assays for such specimens [15, 16]. Therefore, it comes as no surprise that decalcification also significantly decreases the performance of next-generation DNA and RNA sequencing [17–20]. To our knowledge, RNA sequencing has not been systematically explored in decalcified samples.

Here we employed targeted and transcriptomic RNA sequencing on a set of mostly FFPE PMT samples, in an attempt to (1) identify potential alternative fusions in PMT without *FN1-FGFR1/FGF1* fusions, with an emphasis on *FN1* and genes coding for the fibroblast growth factors and fibroblast growth factor receptors; (2) validate the previously obtained positive FISH results and characterize the fusion junctions; and (3) test the utility of AMP-based RNA-sequencing technique (AMP-seq) in decalcified samples. Meanwhile, with the gene expression data thereby generated, we set to analyze the differential expression of Klotho among different groups.

Materials and methods

Tumor samples

FFPE samples of 34 previously reported PMT diagnosed between 1997 and 2019 were collected from the archives of National Taiwan University Hospital (Taipei, Taiwan) and Mayo Clinic (Rochester, MN, USA), as well as the

consultation files of the authors (ALF and J-CL). The cases included 14 with *FN1-FGFR1* fusion revealed by FISH (Group A, with two later reclassified as Group C; see below), 2 with *FN1-FGF1* fusion (Group B), 10 with neither fusion (Group C), and 8 with unknown fusion status (Group D, where FISH analysis had failed) [9]. One case (PMT-72) also had snap-frozen tissue. PMT-61 is one of the 2 PMT from a patient with congenital hypophosphatemic rickets associated with a germline translocation resulting in *KL* overexpression [9, 10]. The clinical and molecular information, as well as the RNA sequencing methods employed, respectively, is summarized in Table 1. This research was approved by the research ethics boards of the respective institutions.

RNA extraction and purification

RNA extraction and purification was performed as previously reported [21]. Briefly, total RNA was extracted with Trizol Reagent (Life Technologies, Carlsbad, CA) for snap-frozen tissue and either RNeasy FFPE kit (Qiagen, Venlo, Netherlands) or Agencourt FormaPure Kit (Beckman Coulter, Brea, CA) for FFPE samples according to the manufacturers' protocols. RNA was quantified with Qubit® RNA HS Assay Kit (Thermo Scientific, Waltham, MA) after purification. Functional RNA quality was assessed in-line with library generation.

AMP-based RNA sequencing and data analysis

A total of 23 samples of PMT were subjected to AMP-seq, implemented as previously described [21]. For library generation, primers targeting *FN1* (as the 5′ partner gene), *KL* (as the 3′ partner gene), and the genes coding for fibroblastic growth factors (FGFs, as 3′ partner genes) and their receptors (FGFRs, chiefly as the 3′ partner genes) were designed using the web-based ArcherDx Custom Assay Designer tool (ArcherDx, Boulder, CO; see Supplementary Table 1 for the list of targeted genes and exons). Overall, 200 ng of RNA as quantified by Qubit was used as input for library generation with the aforementioned gene-specific primers using Archer FusionPlex Protocol for Illumina, revision LA135.C. RNA quality was assessed in-line with library generation by the PreSeq RNA QC qPCR Assay (ArcherDX), provided with the FusionPlex kit, according to kit protocol. Libraries were then sequenced on an Illumina NextSeq 500 using NextSeq 500 v2 reagents (Illumina, San Diego, CA) for paired-end, 150 base pair reads and dual index reads. Housekeeping genes *CHMP2A*, *GPI*, *RAB7A*, and *VCP* were assayed in addition to candidate fusion transcripts as a positive control, using the primers from Archer PreSeq RNA QC Assay.

Table 1 The clinical and molecular features of the study groups

	Case #	Age	Sex	Tumor location	Tissue type	TIO/HPS	FGF23 production[b]	Previous RNA-seq results[c]	Previous FISH	RNA-seq in the present study
Group A	PMT-1	44	M	Thigh	Soft tissue	Present	Positive	*FN1 (23)—FGFR1 (3,4)*	*FN1-FGFR1*	AMP-seq
	PMT-2	57	F	Thigh	Soft tissue	Present	Positive	*FN1 (22)—FGFR1 (3,4)*	*FN1-FGFR1*	AMP-seq
	PMT-18	35	F	Perivertebral	Soft tissue	Present	NP	NP	*FN1-FGFR1*	AMP-seq
	PMT-19	26	M	Thumb	Soft tissue	NP	Positive	NP	*FN1-FGFR1*	NP
	PMT-38	NP	NP	NP	NP	Present	Positive	NP	*FN1-FGFR1*	AMP-seq
	PMT-41	NP	NP	Lung (metastatic)	From soft tissue	Present	Positive	NP	*FN1-FGFR1*	AMP-seq
	PMT-42	NP	NP	NP	NP	Present	Positive	NP	*FN1-FGFR1*	NP
	PMT-63	51	M	Tibia	Bone	Present	NP	NP	*FN1-FGFR1*	AMP-seq
	PMT-64	49	M	Maxillary sinus	Soft tissue	Present	Positive	NP	*FN1-FGFR1*	AMP-seq
	PMT-75	63	F	Thigh	Soft tissue	NP	Positive	NP	*FN1-FGFR1*	NP
	PMT-79	25	M	Heel	Soft tissue	Present	Positive	NP	*FN1-FGFR1*	NP
	PMT-81	55	M	Hip	Soft tissue	NP	Positive	NP	*FN1-FGFR1*	NP
Group B	PMT-31	52	M	Femur	Bone	Present	Positive	NP	*FN1-FGF1*	AMP-seq
	PMT-50	55	F	Femur & pelvis	Bone	Present	Positive	*FN1 (24)—FGF1 (2)*	*FN1-FGF1*	AMP-seq
Group C	PMT-8[d]	48	F	Femur	Bone	Present	Positive	NP	Borderline[d]	RNA exome
	PMT-10[d]	69	M	Foot	Soft tissue	NP	Positive	NP	Borderline[d]	AMP-seq, RNA exome
	PMT-13	62	F	Thigh	Soft tissue	Present	Positive	NP	Negative	AMP-seq
	PMT-15	47	M	Shoulder	Soft tissue	Present	Positive	NP	Negative	NP
	PMT-34	62	F	Femur	Bone	Present	Positive	NP	Negative	AMP-seq
	PMT-44	NP	NP	NP	NP	Present	Positive	NP	Negative	AMP-seq
	PMT-52	48	M	Sinonasal tract	Soft tissue	Present	Positive	NP	Negative	AMP-seq
	PMT-61[a]	30	F	Mastoid	Bone	Present	Positive	NP	Negative	AMP-seq
	PMT-68	60	M	Mandible	Bone	Present	NP	NP	Negative	NP
	PMT-72	53	F	Femur	Bone	Present	Positive	NP	Negative	Transcriptomic RNA-seq
	PMT-73	NP	F	Vulva	Soft tissue	NP	Positive	NP	Negative	RNA exome
	PMT-74	57	M	Buttock	Soft tissue	Present	Positive	NP	Negative	RNA exome
Group D	PMT-25	39	F	Humerus	Bone	Present	Positive	NP	Failed	AMP-seq
	PMT-26	50	M	Femur	Bone	Present	Positive	NP	Failed	AMP-seq
	PMT-27	57	F	Ilium	Bone	Present	Positive	NP	Failed	AMP-seq
	PMT-28	35	M	Femur	Bone	Present	NP	NP	Failed	AMP-seq
	PMT-46	NP	NP	NP	Bone	Present	Positive	NP	Failed	AMP-seq
	PMT-48	NP	NP	NP	NP	Present	Positive	NP	Failed	AMP-seq
	PMT-51	49	M	Femur	Bone	Present	NP	NP	Failed	AMP-seq
	PMT-58[e]	54	F	Ischium	Bone	Present	Positive	NP	Failed	AMP-seq

AMP-seq anchored multiplex PCR-based RNA sequencing (ArcherDx), *CISH* chromogenic in situ hybridization, *FISH* fluorescence in situ hybridization, *NP* not present/performed (including unknown), *RNA-seq* RNA sequencing, *TIO/HPS* tumor-induced osteomalacia and/or hypophosphatemic syndrome

[a]With germline rearrangement upstream of the *KL* gene associated with systemic α-klotho overexpression

[b]By serum analysis or *FGF23* mRNA chromogenic in situ hybridization

[c]Numbers in parentheses indicate exons flanking the fusion junctions

[d]PMT-8 and PMT-10 showed borderline positivity in *FN1-FGFR1* FISH study (juxtaposed signals present in 10–15% of nuclei) and were later reclassified as Group C after reappraisal of the FISH results

[e]PMT-58 underwent liver metastasis (PMT-58–2) during the conduction of this study, which was confirmed to be fusion-negative by FISH, and was therefore reclassified as Group C

Data were analyzed by Archer Analysis version 6.0. Briefly, consensus sequences were compared with known fusion transcripts in the Quiver database of fusions, and novel transcripts were BLASTed to the reference genome guided by RefSeq. A set of filters were applied to the annotated results to reduce false positives. For gene

expression profiling, the unique RNA reads for each gene-specific primer (GSP2) were normalized to the average reads of the four housekeeping genes as mentioned above. The normalized expression data were then retrieved from the Archer Analysis website for heat map generation. The average of expression levels derived from all GSP2 primers targeting any given gene of interest served as the representative expression level of that gene for the comparative purpose; the GSP2 which yielded zero expression level across all tumors were excluded. Mann–Whitney U test was performed to determine the significance of differential expression of the gene(s) of interest between groups, with the cutoff significance level defined as 0.05.

Exome-captured and whole-transcriptomic RNA sequencing and data analysis

Exome-captured and whole-transcriptomic RNA sequencing experiments were performed as previously described [22]. Briefly, RNA was subjected to library construction with the TruSeq RNA Exome kit for exonic region enrichment (Illumina, San Diego, CA, USA) for FFPE samples and TruSeq RNA Sample Prep Kit for poly-A selection for the snap-frozen sample. mRNA sequencing was then performed using a Nextseq or Hiseq system for FFPE or frozen tissue RNA, respectively, for 150-bp paired-end sequencing following the manufacturers' instructions. The yielded read files (in FASTQ format) were mapped to the hg19 reference by STAR for fusion detection, with the gene expression levels calculated by RSEM [23, 24]. Differential genes were identified by R package using DESeq2 [25].

Validation of genomic fusion junction

Genomic DNA was extracted from the FFPE tissue of selective case(s) as previously described [8]. Primers were designed to target the intronic regions in which the genomic fusion junction was presumed to be located (see Supplementary Table 2 for primer sequences). PCR and bidirectional Sanger sequencing were performed as described [8].

RNA chromogenic in situ hybridization (RNAscope) validation of *KL* and *KLB* expression

For semi-quantification of *KL* expression, non-decalcified FFPE tissue slides recently (<7 days) cut from tissue blocks or preserved at −80 °C immediately after tissue sectioning were subjected to RNA CISH. The RNAscope 2.5 HD Detection kit (ACDbio, Newark, CA) was used following the manufacturer's instructions as previously described [26]. Briefly, 5-micron-thick tissue sections were deparaffinized and pretreated with heat and protease before hybridization with *KL, KLB,* and *PPIB* (control) probes, respectively. RNAscope 2.5 Brown (ACDbio) was used for signal amplification and detection chemistry, followed by counterstaining with hematoxylin. Scoring was performed according to the manufacturer's recommendation (0: <1 dot/cell; 1+: 1–3 dots/cell; 2+: 4–9 dots/cell; 3+: 10–15 dots/cell or if <10% dots were in clusters; 4+: >15 dots/cell or if >10% dots were in clusters). The result was deemed inadequate for assessment if the control probe yielded a score of 0.

Results

Evaluation of RNA quality for AMP-based sequencing

PreSeq Cq-values were determined in all but five cases (all belonging to Group D; Table 2). The Cq-values ranged from 26.11 to 34.56 (median: 30.64) and significantly correlated with sample ages ($r = 0.808$ and $P = 3.3 \times 10^{-18}$; Fig. 1a). All the three Group D cases studied had Cq-values greater than 31 and erred on the upper side of the regression line.

In addition, the actual numbers of RNA reads derived from sequencing ranged from 4K to 1171K (median: 807K; Table 2 and Fig. 1b). With the highest number and the lowest number excluded as outliers, the median read number minus twice the standard deviation was arbitrarily defined as the quality threshold (220K). Three cases had RNA read numbers lower than this threshold, including the two oldest specimens (sampled 19 and 17 years ago, respectively) and two Group D bone tumors. These three cases were considered having significantly worse RNA quality than the other cases, and hence a higher probability of falsely negative results.

Further, Group D as a whole had significantly lower RNA reads compared with the other groups (median: 505K vs. 923K, Student's *t* test $P = 0.005$). In addition, the ages of the samples negatively correlated with RNA read numbers ($r = -0.684$ and $P = 1.34 \times 10^{-10}$; Fig. 1c), and this held true when cases of Group D and the other groups were considered separately (for Group D, $r = -0.637$ and $P = 4.93 \times 10^{-8}$; for the others, $r = -0.581$ and $P = 1.63 \times 10^{-9}$).

Fusion genes detected by AMP-based sequencing

Of the eight Group A cases, the results of AMP-seq were consistent with those of FISH in 6, showing in-frame *FN1-FGFR1* fusion transcripts (Table 2). The exact fusion junctions of PMT-1 and PMT-2 were identical to those having been demonstrated by whole-transcriptome

Table 2 Results of AMP-based RNA sequencing (ArcherDx)

PMT#	Group[e]	Sample age (year)	Cq value	RNA reads (×10³)	% RNA/total reads	Fusion junction[a]	Alternative junction[a]	Number of unique start sites supporting the fusion junction[b]	Number of unique supporting reads[b]
PMT-1	A	4	29.61	921	67.4	*FN1 (23)—FGFR1 (3)*	*FN1 (23)—FGFR1 (4)*	24 (76)	118 (427)
PMT-2	A	3	28.60	929	66.5	*FN1 (22)—FGFR1 (3)*	*FN1 (22)—FGFR1 (4)*	37 (56)	218 (173)
PMT-18	A	17	33.03	145	12.9	NP	NP	—	—
PMT-38	A	9	31.36	1171	68.4	*FN1 (23)—FGFR1 (3)*	*FN1 (23)—FGFR1 (4)*	29 (78)	215 (730)
PMT-41	A	7	31.54	893	61.0	*FN1 (16)—FGFR1 (4)*	NP	63	195
PMT-63	A	1	26.11	965	74.2	*FN1 (24)—FGFR1 (3)*	*FN1 (24)—FGFR1 (4)*	333 (355)	3938 (1673)
PMT-64	A	0	26.04	923	73.5	*FN1 (23)—FGFR1 (9)*	*FN1 (23)—FGFR1 (9)*[c]	128 (10)	1070 (11)
PMT-31	B	11	34.56	347	37.9	*FN1 (23)—FGF1 (2)*	NP	9	71
PMT-50	B	1	28.51	1036	71.6	*FN1 (24)—FGF1 (2)*	*FN1 (24)—FGF1 (2)*	120 (78)	1001 (281)
PMT-10	A>C	3	27.40	969	66.6	NP	NP	—	—
PMT-13	C	9	31.19	738	60.0	NP	NP	—	—
PMT-34	C	6	30.13	867	74.1	NP	NP	—	—
PMT-44	C	7	31.17	685	61.3	NP	NP	—	—
PMT-52	C	3	28.74	979	75.1	NP	NP	—	—
PMT-61	C	2	26.82	935	77.6	NP	NP	—	—
PMT-25	D	1	NP	559	33.5	NP	NP	—	—
PMT-26	D>B	7	33.09	623	56.4	*FN1 (26)—FGF1 (2)*	NP	7	16
PMT-27	D	6	NP	24	2.8	*THRB (11)*[d]*—FGF10 (1)*	NP	4	18
PMT-28	D	19	NP	4	69.2	NP	NP	—	—
PMT-46	D	8	NP	451	64.4	NP	NP	—	—
PMT-48	D	7	NP	353	37.5	NP	NP	—	—
PMT-51	D	7	33.73	595	56.6	NP	NP	—	—
PMT-58	D>C	4	31.14	807	74.9	NP	NP	—	—

NP not present/performed

[a]Numbers in parentheses indicate exons flanking the fusion junctions, and alternative junctions indicate shorter fusion products

[b]Numbers in parentheses indicate alternative junctions

[c]67 bp into *FGFR1* exon 9, immediately 3' to an "AG" sequence

[d]3' UTR

[e]PMT-10, PMT-26, and PMT-58 were reclassified as Group C, B, and C because of revised FISH results, identification of *FN1-FGF1* fusion by AMP-seq, and a metastatic hepatic tumor (PMT-58-2) later confirmed to be fusion-negative by FISH, respectively
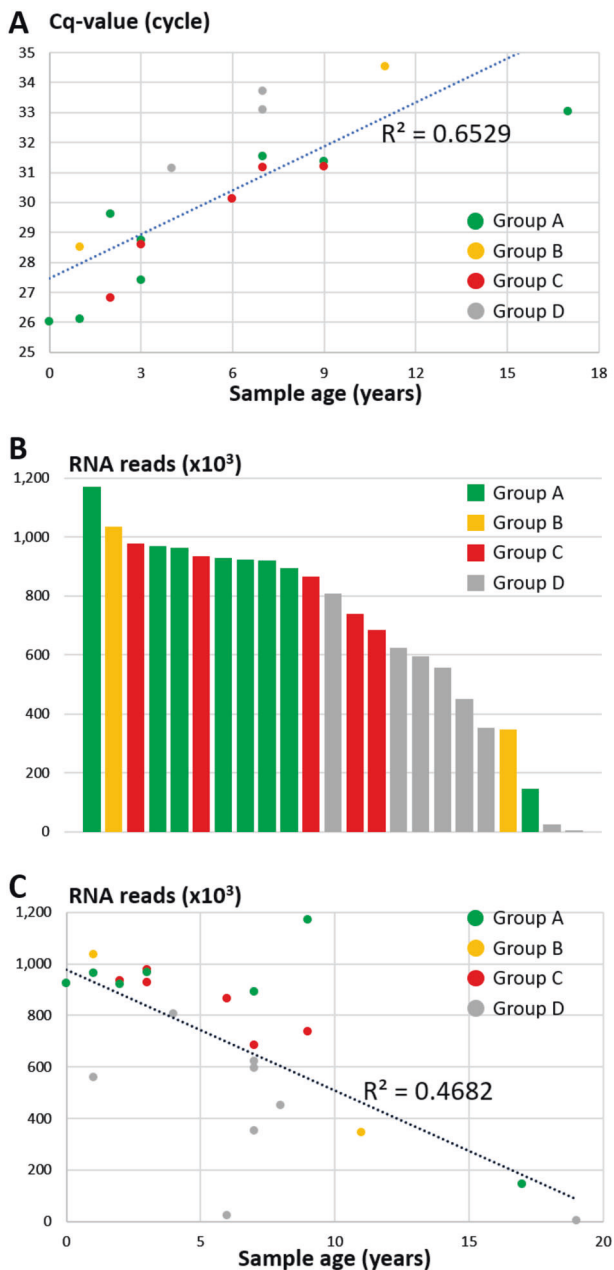
Fig. 1 Parameters of AMP-seq reflecting the RNA quality. The Cq-values correlate with sample ages (**a**); the Group D (decalcified) cases err on the upper side of the regression line. RNA read numbers in relation to sample group (**b**) and sample age (**c**). Samples with lower read numbers are enriched by Group D cases

sequencing previously [8]. The breakpoints of *FN1* rested on the 3′ ends of exon 16, 22, 23, and 24 in 1, 1, 3, and 1 cases, respectively. For the *FGFR1* gene, breakpoints at the 5′ end of exon 3 were detected in four cases, all of which had concomitant transcripts with an exon 4 fusion junction that probably represented alternative splicing as previously suggested [8]. PMT-41 had exon 4 as the sole *FGFR1* breakpoint, implying a genomic breakpoint in intron 3. It is

noteworthy that PMT-64 harbored the fusion transcripts with novel breakpoints in *FGFR1* exon 9, either at the 5′ end or, as a minor variant, 67 bp into the exon (immediately 3′ to an "AG" sequence, supposedly a de novo splice acceptor).

Both Group B cases were confirmed to have in-frame *FN1-FGF1* fusions, with exons 23 and 24 of *FN1*, respectively, fused to exon 2 of *FGF1* at the nucleotide immediately 3′ to an "AG" sequence. The fusion junction of PMT-50 was identical to that previously demonstrated by RNA sequencing [9].

Two Group D bone tumors contained detectable fusions. PMT-26 harbored an in-frame *FN1-FGF1* fusion with the fusion junction identical to that identified in PMT-16 (exon 26 to exon 2)[9] and therefore was reclassified as Group B ("D > B"). PMT-27 had a novel *THRB-FGF10* fusion, with the breakpoints located in the 3′ UTR of *THRB* (coding for thyroid hormone receptor beta) and at the 104th nucleotide into the coding sequence of *FGF10*, respectively; the significance of this fusion is uncertain, as the *FGF10* part is not predicted to be translated into peptide in the form of chimeric protein. RT-PCR to validate the fusions in both cases failed, probably because of previous tissue decalcification (data not shown). None of the Group C cases had a detectable fusion. The results of AMP-based sequencing are summarized in Table 2 and Supplementary Table 3.

Confirmation of genomic fusion junction and clinicopathologic review of PMT-64

In contrast to all other *FGFR1* breakpoints we have so far identified in PMT, which are located 5′ to exon 3, 4, or 5 and thus include at least two receptor domains of FGFR1 in the chimeric protein, PMT-64 had a breakpoint in exon 9, which included the transmembrane domain and a minimal extracellular part (47 bp) of FGFR1. To exclude the possibility of this unusual fusion junction representing alternative splicing rather than reflecting the true genomic junction, genomic DNA PCR and Sanger sequencing was performed and confirmed the genomic breakpoint in *FN1* intron 23 and *FGFR1* intron 8 (Fig. 2a). The predicted chimeric protein domains are shown in Fig. 2b.

The exceptional fusion junction of this case prompted us to look for its clinical and pathological difference from the other cases. The tumor manifested itself with classical TIO/hypophosphatemia and was resected from the left maxillary sinus of a 49-year-old man. It was one of the only four sinonasal cases we have reported, with the other three cases harboring neither fusion [9]. Histologically, the tumor exhibited typical features of PMT, consisting of spindled cells with bland nuclei and eosinophilic cytoplasm, in a richly vascularized and collagenous stroma interspersed
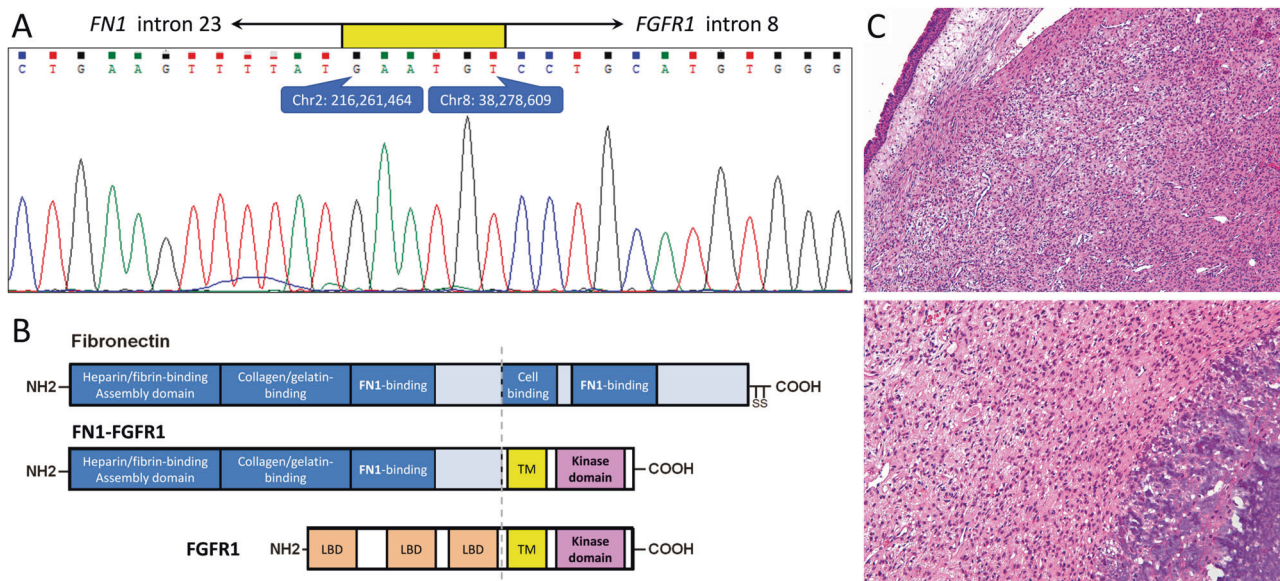
Fig. 2 Molecular and pathologic features of PMT-64. **a** The sequence flanking the genomic fusion junction. **b** The presumed fusion protein contains no ligand-binding domain (LBD) of FGFR1. **c** The histology is typical of PMT

with prominent foci of so-called 'grungy' calcifications (Fig. 2c). Like many other PMTs, it was immunoreactive for FGFR1 and FGF1 and positive for *FGF23* mRNA by chromogenic in situ hybridization [9]. The clinicopathological features of this case were essentially identical to those of PMT showing more conventional fusion junctions.

Reappraisal of the FISH results of the inconsistent or borderline cases

The discrepancy between previous FISH and the current AMP-seq results in PMT-10 and PMT-18 prompted us to review the FISH data of both cases as well as two other cases with borderline FISH results. PMT-18 was a 17-year-old sample and, despite a convincingly positive *FN1-FGFR1* FISH result, in retrospect had an RNA quality among the worst of this cohort, to which a falsely negative sequencing result might be attributed. On the other hand, PMT-10, as well as PMT-8 and PMT-9, was originally classified as Group A based on borderline positive FISH results (10–15% of cells harboring a fusion signal, i.e., a 5′ *FN1* signal and a 3′ *FGFR1* signal less than half the average width of a signal apart, after meticulously counting >200 cells) [8]. Nonetheless, based on our later experience, cases positive for *FN1-FGFR1* fusion usually have cells more readily found to have a fusion signal where the two constituent signals just abut or even overlap with each other, instead of being slightly separate as was observed in the three borderline cases in retrospect. Therefore, PMT-8,

PMT-9 (not included in this study), and PMT-10 were reclassified as Group C, where the occasional juxtaposition of *FN1* and *FGFR1* signals observed by FISH probably represented fortuitous proximity (i.e., falsely positive results).

Exome-captured and whole-transcriptomic RNA sequencing confirmed the fusion-negative status of selective Group C cases

To cross-validate their fusion status, PMT-8 and PMT-10, as well as three additional Group C cases, were subjected to RNA exome sequencing ($N = 4$) or transcriptomic sequencing ($N = 1$). Consistent with the results of FISH analysis/reappraisal and AMP-seq (in the case of PMT-10), no *FN1-FGFR1/FGF1* or other convincing fusion could be identified in any of the five cases (data not shown). Collectively, these RNA sequencing data suggested fundamentally different mechanisms might be responsible for PMT without *FN1-FGFR1/FGF1* fusion.

Group C showed significantly higher *KL* or *KLB* expression

The heat map of gene expression profiles derived from AMP-seq is illustrated as Supplementary Fig. 1. Five cases with the lowest total RNA reads and/or zero expression of all four control genes were excluded from the analysis because of the inferred poor sample quality. In keeping with our previous observations, *FN1*, *FGFR1*, *FGF1*, and
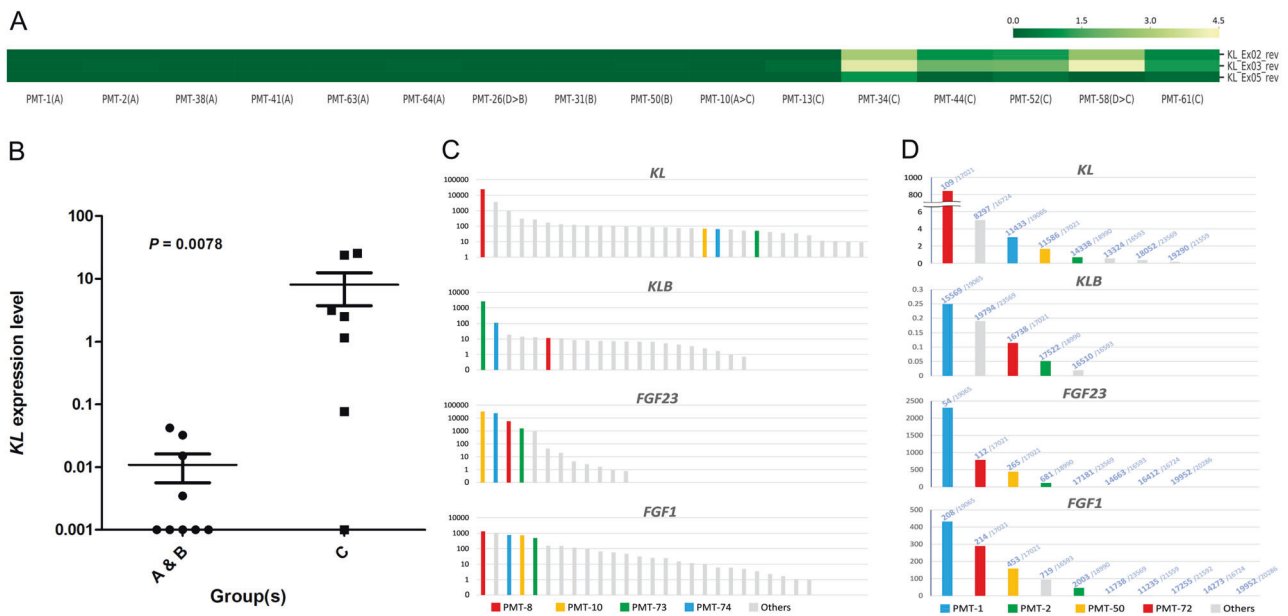
Fig. 3 Differential expression of *KL* and *KLB* in various groups of PMT and non-PMT mesenchymal tumors by cross-platform RNA sequencing. **a**, **b** The *KL* expression levels derived from the three primers by AMP-seq are significantly higher in Group C than Groups A and B combined. The expression level of zero was reassigned as 0.001 for $\log_e$ transformation. PMT-26 was reclassified as Group B ("D > B") based on the AMP-seq results; PMT-10 was reclassified as Group C ("A > C") after revisiting the previous FISH data; PMT-58 was reclassified as Group C ("D > C") because a metastatic hepatic tumor (PMT-58-2) was later confirmed to be fusion-negative by FISH. **c** Three additional Group C PMT, PMT-8, PMT-73, and PMT-74, expressed the highest levels of *KL* or *KLB* (in normalized count) among the 30 mesenchymal tumors subjected to the RNA exome sequencing ("Others" indicates non-PMT tumors). **d** An additional Group C PMT (PMT-72) exhibited the highest level of *KL* (in FPKM) among the 10 mesenchymal tumors with snap-frozen tissue subjected to whole-transcriptomic sequencing ("Others" indicates non-PMT tumors). All the other tumors revealed very low *KL* and *KLB* expression, including the three fusion-containing PMT. The numbers on top of each bar represent the rank of gene expression /total number of expressed genes of respective tumor

FGF23 were the most constantly expressed genes across all tumor groups.

Of note, Group C tumors, including PMT-61 which was a case of germline rearrangement-induced systemic *KL* upregulation [10], expressed significantly higher levels of *KL* by AMP-seq in comparison with Groups A and B combined ($P = 0.0078$; Fig. 3a, b). During the conduction of this study, patient of PMT-58 developed a metastatic PMT to the liver (PMT-58-2), where FISH revealed no *FN1-FGFR1/FGF1* fusion (data not shown), and therefore PMT-58 was reclassified as Group C ("D > C"). By AMP-seq, PMT-58 also expressed a high level of *KL* (Fig. 3a).

By RNA exome and whole-transcriptomic sequencing, respectively, two additional Group C cases were also found to express high levels of *KL* (Fig. 3c, d). Two other Group C cases, despite showing low *KL* expression, presented the highest levels of *KLB* instead among the 30 mesenchymal tumors analyzed with the same platform (i.e., RNA exome; Fig. 3c) [22]. Taken together, four of the five fusion-negative PMT (except PMT-10) expressed the highest levels of either *KL* or *KLB* among the 40 PMT or non-PMT mesenchymal tumors, while both genes were barely expressed in the fusion-positive PMT [8, 9], in keeping with the AMP-seq results. Parenthetically, our data also showed that PMT tended to express higher levels of selective genes related to osteoblast/osteocyte or osteoclast, similar to the findings of a previous report (Fig. 3c, d, and Supplementary Fig. 2) [27].

To further validate these findings, RNAscope was performed to semi-quantify *KL* and *KLB* RNA expression. Adequate samples were available in 11 Group A, 1 Group B, and 10 Group C cases (Table 1). Three samples failed the RNAscope analysis with zero expression of the control gene (and *KL/KLB*). Consistent with the AMP-seq results, the Group C cases expressed significantly higher levels of *KL* in comparison with Groups A and B combined ($P = 0.0208$) (Fig. 4a, b). Moreover, the *KL* expression levels derived from RNAscope and AMP-seq (ArcherDx) were highly correlated [RNAscope vs. log(ArcherDx): regression $r^2 = 0.822$, $P = 2.98 \times 10^{-4}$; Spearman $r = 0.8847$, $P = 0.0011$], which could serve as a mutual validation of the credibility of both platforms in the characterization of gene expression (Fig. 4c). Furthermore, two of the four *KL*-negative Group C cases (PMT-73 and PMT-74) expressed the highest levels of *KLB*, consistent with their RNA exome
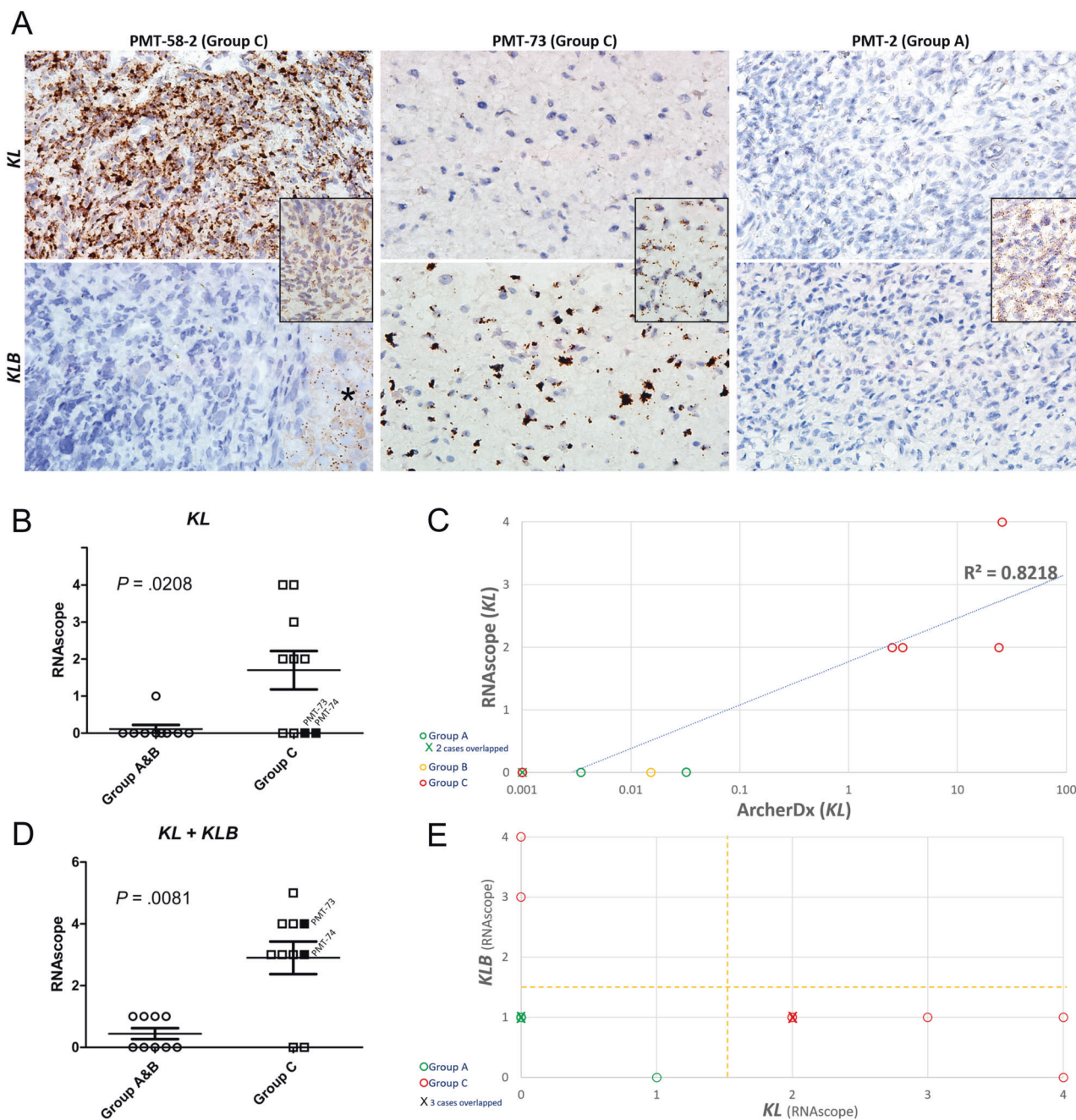
Fig. 4 RNA CISH (RNAscope) to detect *KL* and *KLB* expression. **a** PMT-58-2 and PMT-73 showed a score of 4 for *KL* and *KLB*, respectively, while PMT-2 was negative for both genes (insets: *PPIB* control). Also, note the normal expression of *KLB* in the adjacent liver tissue in PMT-58-2 (asterisk). **b** Group C as a whole expressed significantly higher levels of *KL* than Groups A and B combined. **c** The *KL* expression levels derived from RNAscope and AMP-seq sequencing results, while the other cases showed zero or merely detectable *KLB* expression (Fig. 4a). The Group C cases demonstrated significantly higher combined *KL/KLB* scores than Groups A and B ($P = 0.0081$; Fig. 4d). Collectively, by RNAscope, 8 of the 10 Group C cases showed (ArcherDx) highly correlated with each other. **d** With two of the *KL*-negative Group C cases (PMT-73 and PMT-74) highly expressing *KLB* instead, Group C also revealed significantly higher sums of *KL* and *KLB* scores compared with Groups A and B. **e** The overexpression (when defined as a score of 2~4) of either gene appeared mutually exclusive (cases with scores of zero in both genes were not shown)

overexpression (defined as a score of 2~4) of either gene in a mutually exclusive manner, in stark contrast with Groups A and B (Fig. 4e).

In summary, these findings suggested that aberrant expression of α-Klotho or β-Klotho might possibly serve as

an alternative to the *FN1-FGFR1/FGF1* fusion genes as a tumorigenesis mechanism in fusion-negative PMT.

Discussion

In prior studies, we have identified *FN1-FGFR1* or *FN1-FGF1* fusion gene in nearly half of PMT cases [8, 9]. As the activated FGFR1 pathway is known for its oncogenic roles in other tumor types and is a canonical driver of FGF23 production in osteocytes, our findings suggest a central role for the FGFR1 pathway in both the tumorigenesis and FGF23 hypersecretion phenotype of PMT, and hence a rationale for FGFR inhibitors to serve as therapeutic agents [28–33]. However, the tumorigenesis mechanisms remain elusive in more than half of PMT which harbor neither fusion gene. It is reasonable to speculate that alternative fusions might be in play, particularly those involving paralogous genes in the FGFR or FGF family as well as the *FN1* gene. In this study, we employed three different RNA-seq techniques to study a large cohort of PMT with a special focus on these paralogous genes and the fusion-negative (Group C) cases. Somewhat to our surprise, none of these tumors were found with an alternative fusion except for the *THRB-FGF10* fusion identified in a previously decalcified (Group D) case, whose significance is uncertain as the *THRB* breakpoint falls in the 3′ UTR. Therefore, the current data suggest the tumorigenic mechanisms behind the PMT without either known fusion gene might be categorically different and probably do not involve genetic fusions, or at least not those detectable at the RNA level.

Rather, as the most important finding of this study, these fusion-negative PMT exhibited significantly higher *KL* or *KLB* expression despite no associated fusion detected. *KL* encodes α-Klotho, an obligatory co-receptor for FGF23-FGFR1 binding, and its expression is mostly limited to renal tubules, choroid plexus, and parathyroid gland [34]. As we previously hypothesized in view of the unique case PMT-61, aberrant expression of α-Klotho in FGF23-secreting cells, such as osteocytes and their precursors, might possibly facilitate the establishment of an FGF23-FGFR1 autocrine loop, which might in turn drive the upregulation of FGF23 and tumorigenesis through the activated FGFR1 pathway, thereby underpinning the formation of PMT [9, 29–33]. Echoing our findings, a subset of PMT with α-Klotho expression was recently reported, although the respective authors failed to characterize the fusion status of their cases, except for 1 case where RNA sequencing also revealed *KL* overexpression and no fusion gene [27, 35]. On the other hand, *KLB*, coding for β-Klotho, is a paralog of *KL*. To our knowledge, there has been no report of β-Klotho expression in PMT. β-Klotho is known as a co-receptor for FGF19/21-FGFR binding [36].

However, the expression of FGF19 and FGF21 was low, if any, in all PMT studied including those overexpressing *KLB*. Therefore, our findings might suggest an unrecognized role for β-Klotho in the binding and expression of FGF23 or FGF1, another frequently overexpressed fibroblast growth factor in PMT. Importantly, the implication of *KL/KLB* overexpression in a majority of fusion-negative PMT suggests the FGFR pathway probably also plays a pivotal role in this group of tumors, hence the potential utility of FGFR inhibitors in treating PMT regardless of their fusion status. The mechanisms behind the upregulation of *KL/KLB* and how they lead to PMT formation remain to be investigated. It is noteworthy that the germline chromosomal rearrangement in the patient with PMT-61 involved a locus 49 kb upstream of *KL*, which cannot be detected at the RNA level [9, 10]. Going forward, it will be interesting to see whether similar mechanisms could have a role in the overexpression of *KL/KLB* in other fusion-negative PMT.

Our transcriptome-wide analyses of PMT also revealed upregulation of osteocyte- or osteoclast-related genes as indicated in a previous study, suggesting the osteoblastic differentiation and a possible role of osteoclast in the tumorigenesis of PMT (Fig. 3c, d and Supplementary Fig. 2) [27]. Of potential interest is *SPP1* (coding for osteopontin), which is involved in osteoclast attachment to bone mineral and a variety of cellular processes including tumorigenesis [37]. While the fusion-negative PMT expressed significantly higher levels of *SPP1* than non-PMT mesenchymal tumors, all the 3 fusion-positive PMT analyzed showed zero expression of this gene (Supplementary Fig. 2). Whether *SPP1* might play differential roles in PMT of different fusion status might warrant further study to determine.

The current study characterized the capability of the AMP-seq to detect fusion transcripts from FFPE samples with highly degraded nucleic acids. In the present series, fusion detection was successful in samples as old as 11 years. Further, we were able to identify *FN1-FGF1* fusion in PMT-26, the decalcification of which had probably caused the failure of previous FISH analyses. To our knowledge, this was the first demonstration of fusion detection by AMP-seq in decalcified samples. Interestingly, all four cases with the *FN1-FGF1* fusion were bone tumors [9], suggesting a possible context/microenvironment-dependence in the tumorigenic mechanism of this fusion. Meanwhile, the current study also clearly demonstrated the limitations of AMP-seq, whose scope of surveillance is confined to a very focused panel of target genes and thus heavily hypothesis-based, and whose performance was obviously compromised by the old sample age and previous tissue decalcification. As shown, the RNA quality demonstrated a significantly reverse relation to these factors.

Similar to our findings, recently Lam *et al.* failed to identify genetic fusion in any decalcified tissue using the same AMP-seq technique and could attribute the suboptimal sequencing quality to the decalcification process *per se* in two cases [20].

Knowledge of the exact fusion junctions derived from RNA sequencing, and hence the inferred protein domains included in the chimeric proteins, is valuable for dissecting the functional aspects of the fusions, which cannot be provided by FISH. In contrast to previously characterized *FN1-FGFR1* fusions, all of which included the ligand-binding domain of FGFR1, implying that the ligand binding might add to the tumorigenic pathway as an autocrine positive feedback loop, the current data have revealed one exception (PMT-64) that does not contain this ligand-binding domain, suggesting that the pathogenesis of PMT may not always be related to ligand binding (Fig. 2b). This finding appears to echo the preliminary observations in a recent phase 2 clinical trial, where a neutralizing anti-FGF23 antibody did not seem to confer a significant tumoricidal anti-PMT effect as shown by an FGFR1 inhibitor [38, 39]. What might be essential instead, in terms of the contribution of FGFR1 (other than its kinase domain) to the chimeric protein, is the transmembrane domain of FGFR1, which could anchor the fusion protein onto a membrane to avoid being secreted, a hypothesis that is supported by the unusual *FGFR1* breakpoints seen in PMT, as opposed to the classical exon 10 breakpoint seen in most other *FGFR1*-rearranged neoplasms [9].

There are limitations of this study. The current panel of gene-specific primers for AMP-seq did not cover *FN1* outside exons 15–30, because *FN1* breakpoints in PMT had been located between exons 22 and 28 when this panel was designed. However, an exon 42 breakpoint was later identified in a calcifying aponeurotic fibroma with *FN1-EGF* fusion and a gastrointestinal leiomyoma with *FN1-ALK* fusion [40, 41], underscoring the insufficient coverage of the current panel and the possibility that some fusion-positive cases might have been overlooked. Furthermore, the *FGF16* gene was inadvertently left out of this panel. Moreover, although the Group C cases were shown to express significantly higher *KL/KLB* at the RNA level by AMP-seq and/or RNA CISH, how the overexpression of the *KL/KLB* mRNA could be translated into the protein level requires further validation.

In conclusion, the current data demonstrated the absence of alternative fusion gene in PMT without *FN1-FGFR1/FGF1* fusion, which might probably harbor significantly distinct aberrations. In particular, the overexpression of Klotho, which was noted in the majority of fusion-negative tumors in stark contrast with those containing either known fusion, could possibly replace those fusion genes as a novel tumorigenic driver by activating the FGFR pathway through enabling an FGF23-FGFR autocrine loop. If proved, this hypothesis would legitimize the utility of FGFR inhibitors to treat those Klotho-overexpressing fusion-negative PMT where necessary. Further studies are required to confirm this phenotype in a larger group of fusion-negative PMT and to characterize the genomic or epigenetic underpinnings.

Compliance with ethical standards

Conflict of interest The authors declare that they have no conflict of interest.

Publisher's note Springer Nature remains neutral with regard to jurisdictional claims in published maps and institutional affiliations.

References

1. Folpe AL. Phosphaturic mesenchymal tumour. In: Fletcher CDM, Bridge JA, Hogendoorn PCW, Mertens F, editors. World Health Organization classification of tumours of soft tissue and bone. 4th ed. Lyon: IARC Press; 2013. p. 211–2.

2. Folpe AL, Fanburg-Smith JC, Billings SD, Bisceglia M, Bertoni F, Cho JY, et al. Most osteomalacia-associated mesenchymal tumors are a single histopathologic entity: an analysis of 32 cases and a comprehensive review of the literature. Am J Surgical Pathol. 2004;28:1–30.

3. Shimada T, Mizutani S, Muto T, Yoneya T, Hino R, Takeda S, et al. Cloning and characterization of FGF23 as a causative factor of tumor-induced osteomalacia. PNAS. 2001;98:6500–5.

4. White KE, Larsson TE, Econs MJ. The roles of specific genes implicated as circulating factors involved in normal and disordered phosphate homeostasis: frizzled related protein-4, matrix extracellular phosphoglycoprotein, and fibroblast growth factor 23. Endocr Rev. 2006;27:221–41.

5. Berndt T, Craig TA, Bowe AE, Vassiliadis J, Reczek D, Finnegan R, et al. Secreted frizzled-related protein 4 is a potent tumor-derived phosphaturic agent. J Clin Investig. 2003;112:785–94.

6. Rowe PS, de Zoysa PA, Dong R, Wang HR, White KE, Econs MJ, et al. MEPE, a new gene expressed in bone marrow and tumors causing osteomalacia. Genomics. 2000;67:54–68.

7. Habra MA, Jimenez C, Huang SC, Cote GJ, Murphy WA Jr., Gagel RF, et al. Expression analysis of fibroblast growth factor-23, matrix extracellular phosphoglycoprotein, secreted frizzled-related protein-4, and fibroblast growth factor-7: identification of fibroblast growth factor-23 and matrix extracellular phosphoglycoprotein as major factors involved in tumor-induced osteomalacia. Endocr Pract Off J Am Coll Endocrinol Am Assoc Clin Endocrinologists. 2008;14:1108–14.

8. Lee JC, Jeng YM, Su SY, Wu CT, Tsai KS, Lee CH, et al. Identification of a novel FN1-FGFR1 genetic fusion as a frequent

event in phosphaturic mesenchymal tumour. J Pathol. 2015;235:539–45.

9. Lee JC, Su SY, Changou CA, Rong-Sen Yang, Keh-Sung Tsai, Collins MT, et al. Characterization of FN1-FGFR1 and Novel FN1-FGF1 fusion genes in a large series of phosphaturic mesenchymal tumors. Mod Pathol. 2016;29:1335–46.

10. Brownstein CA, Adler F, Nelson-Williams C, Iijima J, Li P, Imura A, et al. A translocation causing increased alpha-klotho level results in hypophosphatemic rickets and hyperparathyroidism. PNAS. 2008;105:3455–60.

11. Xuan J, Yu Y, Qing T, Guo L, Shi L. Next-generation sequencing in the clinic: promises and challenges. Cancer Lett. 2013;340:284–95.

12. Cieslik M, Chugh R, Wu YM, Wu M, Brennan C, Lonigro R, et al. The use of exome capture RNA-seq for highly degraded RNA with application to clinical cancer sequencing. Genome Res. 2015;25:1372–81.

13. Wu G, Barnhill RL, Lee S, Li Y, Shao Y, Easton J, et al. The landscape of fusion transcripts in spitzoid melanoma and biologically indeterminate spitzoid tumors by RNA sequencing. Mod Pathol. 2016;29:359–69.

14. Zheng Z, Liebers M, Zhelyazkova B, Cao Y, Panditi D, Lynch KD, et al. Anchored multiplex PCR for targeted next-generation sequencing. Nat Med. 2014;20:1479–84.

15. Singh VM, Salunga RC, Huang VJ, Tran Y, Erlander M, Plumlee P, et al. Analysis of the effect of various decalcification agents on the quantity and quality of nucleic acid (DNA and RNA) recovered from bone biopsies. Ann Diagn Pathol. 2013;17:322–6.

16. Schrijver WA, van der Groep P, Hoefnagel LD, Ter Hoeve ND, Peeters T, Moelans CB, et al. Influence of decalcification procedures on immunohistochemistry and molecular pathology in breast cancer. Mod Pathol. 2016;29:1460–70.

17. Chen H, Luthra R, Goswami RS, Singh RR, Roy-Chowdhuri S. Analysis of pre-analytic factors affecting the success of clinical next-generation sequencing of solid organ malignancies. Cancers (Basel). 2015;7:1699–715.

18. Zheng G, Lin MT, Lokhandwala PM, Beierl K, Netto GJ, Gocke CD, et al. Clinical mutational profiling of bone metastases of lung and colon carcinoma and malignant melanoma using next-generation sequencing. Cancer. 2016;124:744–53.

19. Goswami RS, Luthra R, Singh RR, Patel KP, Routbort MJ, Aldape KD, et al. Identification of factors affecting the success of next-generation sequencing testing in solid tumors. Am J Clin Pathol. 2016;145:222–37.

20. Lam SW, Cleton-Jansen AM, Cleven AHG, Ruano D, van Wezel T, Szuhai K, et al. Molecular analysis of gene fusions in bone and soft tissue tumors by anchored multiplex PCR-based targeted next-generation sequencing. J Mol Diagn. 2018;20:653–63.

21. Li X, Anand M, Haimes JD, Manoj N, Berlin AM, Kudlow BA, et al. The application of next-generation sequencing-based molecular diagnostics in endometrial stromal sarcoma. Histopathology. 2016;69:551–9.

22. Lee CH, Kao YC, Lee WR, Hsiao YW, Lu TP, Chu CY, et al. Clinicopathologic characterization of GREB1-rearranged uterine sarcomas with variable sex-cord differentiation. Am J surgical Pathol. 2019;43:928–42.

23. Dobin A, Davis CA, Schlesinger F, Drenkow J, Zaleski C, Jha S, et al. STAR: ultrafast universal RNA-seq aligner. Bioinformatics. 2013;29:15–21.

24. Li B, Dewey CN. RSEM: accurate transcript quantification from RNA-Seq data with or without a reference genome. BMC Bioinf. 2011;12:323.

25. Love MI, Huber W, Anders S. Moderated estimation of fold change and dispersion for RNA-seq data with DESeq2. Genome Biol. 2014;15:550.

26. Carter JM, Caron BL, Dogan A, Folpe AL. A novel chromogenic in situ hybridization assay for FGF23 mRNA in phosphaturic mesenchymal tumors. Am J Surgical Pathol. 2015;39:75–83.

27. Kinoshita Y, Takashi Y, Ito N, Ikegawa S, Mano H, Ushiku T, et al. Ectopic expression of Klotho in fibroblast growth factor 23 (FGF23)-producing tumors that cause tumor-induced rickets/osteomalacia (TIO). Bone Rep. 2019;10:100192.

28. Parker BC, Engels M, Annala M, Zhang W. Emergence of FGFR family gene fusions as therapeutic targets in a wide spectrum of solid tumours. J Pathol. 2014;232:4–15.

29. White KE, Cabral JM, Davis SI, Fishburn T, Evans WE, Ichikawa S, et al. Mutations that cause osteoglophonic dysplasia define novel roles for FGFR1 in bone elongation. Am J Hum Genet. 2005;76:361–7.

30. Liu S, Tang W, Fang J, Ren J, Li H, Xiao Z, et al. Novel regulators of Fgf23 expression and mineralization in Hyp bone. Mol Endocrinol. 2009;23:1505–18.

31. Martin A, Liu S, David V, Li H, Karydis A, Feng JQ, et al. Bone proteins PHEX and DMP1 regulate fibroblastic growth factor Fgf23 expression in osteocytes through a common pathway involving FGF receptor (FGFR) signaling. FASEB J. 2011;25:2551–62.

32. Wu AL, Feng B, Chen MZ, Kolumam G, Zavala-Solorio J, Wyatt SK, et al. Antibody-mediated activation of FGFR1 induces FGF23 production and hypophosphatemia. PLoS One. 2013;8:e57322.

33. Xiao Z, Huang J, Cao L, Liang Y, Han X, Quarles LD. Osteocyte-specific deletion of Fgfr1 suppresses FGF23. PLoS One. 2014;9:e104154.

34. Nabeshima Y. Klotho: a fundamental regulator of aging. Ageing Res Rev. 2002;1:627–38.

35. Yavropoulou MP, Gerothanasi N, Frydas A, Triantafyllou E, Poulios C, Hytiroglou P, et al. Tumor-induced osteomalacia due to a recurrent mesenchymal tumor overexpressing several growth factor receptors. Endocrinol Diabetes Metab Case Rep. 2015; 2015:150025.

36. Kurosu H, Choi M, Ogawa Y, Dickson AS, Goetz R, Eliseenkova AV, et al. Tissue-specific expression of betaKlotho and fibroblast growth factor (FGF) receptor isoforms determines metabolic activity of FGF19 and FGF21. J Biol Chem. 2007; 282:26687–95.

37. Zhao H, Chen Q, Alam A, Cui J, Suen KC, Soo AP, et al. The role of osteopontin in the progression of solid organ tumour. Cell Death Dis. 2018;9:356.

38. Miller CB, Bergwitz C, Blau J, Boyce A, Gafni RI, Guthrie L, et al. Response of tumor-induced osteomalacia (TIO) to the FGFR inhibitor BGJ398. J Clin Oncol Off J Am Soc Clin Oncol. 2016;34:e22500–e.

39. DeBeur SJ, Miller PD, Weber TJ, Peacock M, Ruppe MD, Insogna K, et al. Effects of burosumab (KRN23), a human monoclonal antibody to FGF23, in patients with tumor-induced osteomalacia (TIO) or epidermal nevus syndrome (ENS) [abstract SU0325]. J Bone Min Res. 2017;32:S280.

40. Puls F, Hofvander J, Magnusson L, Nilsson J, Haywood E, Sumathi VP, et al. FN1-EGF gene fusions are recurrent in calcifying aponeurotic fibroma. J Pathol. 2016;238:502–7.

41. Panagopoulos I, Gorunova L, Lund-Iversen M, Lobmaier I, Bjerkehagen B, Heim S. Recurrent fusion of the genes FN1 and ALK in gastrointestinal leiomyomas. Mod Pathol. 2016;29: 1415–23.

Affiliations

Cheng-Han Lee[1] · Sheng-Yao Su[2,3] · Kesavan Sittampalam[4] · Paul Chih-Hsueh Chen[5] · Fredrik Petersson[6] ·
Yu-Chien Kao[7] · Thomas O. Carpenter[8] · Tsung-Han Hsieh[9] · Eiichi Konishi[10] · Jen-Wei Tsai[11] · Steven D. Billings[12] ·
Andrew L. Folpe[13] · Jen-Chieh Lee ●[14]

[1] Department of Laboratory Medicine and Pathology, University of Alberta and Royal Alexandra Hospital, Edmonton, AB, Canada

[2] Institute of Information Science, Academia Sinica, Taipei, Taiwan

[3] Bioinformatics Program, Taiwan International Graduate Program, Academia Sinica & Institute of Biomedical Informatics, National Yang-Ming University, Taipei, Taiwan

[4] Pathology Department, Singapore General Hospital, Singapore, Singapore

[5] Department of Pathology, National Yang-Ming University and Taipei Veterans General Hospital, Taipei, Taiwan

[6] Department of Pathology, National University Health System, Singapore, Singapore

[7] Department of Pathology, Shuang Ho Hospital, Taipei Medical University, Taipei, Taiwan

[8] Department of Pediatrics (Endocrinology), Yale University School of Medicine, New Haven, CT, USA

[9] Joint Biobank, Office of Human Research, Taipei Medical University, Taipei, Taiwan

[10] Department of Pathology, Kyoto Prefectural University of Medicine, Kyoto, Japan

[11] Department of Pathology, E-DA Hospital, I-Shou University, Kaohsiung, Taiwan

[12] Department of Pathology, Cleveland Clinic, Cleveland, OH, USA

[13] Department of Laboratory Medicine and Pathology, Mayo Clinic, Rochester, MN, USA

[14] Department and Graduate Institute of Pathology, National Taiwan University Hospital, National Taiwan University College of Medicine, Taipei, Taiwan